

AN IMMERSED BOUNDARY METHOD FOR COMPUTING HEAT AND FLUID FLOW IN POROUS MEDIA

David J. Lopez Penha*, Lilya Ghazaryan*, Bernard J. Geurts^{*,†},
Steffen Stolz^{††,*} and Markus Nordlund^{††}

*Multiscale Modeling & Simulation, Dept. of Applied Mathematics, University of Twente,
P.O. Box 217, 7500 AE Enschede, The Netherlands.

e-mail: {d.j.lopezpenha, l.ghazaryan, b.j.geurts}@utwente.nl

[†]Anisotropic Turbulence, Dept. of Applied Physics, Eindhoven University of Technology,
P.O. Box 513, 5600 MB Eindhoven, The Netherlands.

^{††}Philip Morris International Research & Development, Philip Morris Products S.A.,
Quai Jeanrenaud 5, 2000 Neuchâtel, Switzerland.
e-mail: {steffen.stolz, markus.nordlund}@pmintl.com

Key words: Immersed boundary method, volume-penalization, porous media, incompressible Navier-Stokes equations, conjugate heat transfer, numerical simulation

Abstract. *A volume-penalizing immersed boundary (IB) method is presented that facilitates the computation of fluid flow in complex porous media. The computational domain is composed of a uniform Cartesian grid, and solid bodies are approximated on this grid using a series of grid cells (i.e., a “staircase” approximation). Solid bodies are distinguished from fluid regions using a binary phase-indicator function: Taking the value of “1” in the solid parts of the domain and “0” in the fluid parts. The effect of solid bodies on the flow is modeled using a source term in the momentum equations. The source term is active only within solid parts of the domain, and enforces the no-slip boundary condition. Fluid regions are governed by the incompressible Navier-Stokes equations. An extension of the IB method is proposed to tackle coupled fluid-solid heat transfer. The extended IB method is validated for Poiseuille flow, which allows for a direct comparison of the numerical results against a closed analytical solution. We subsequently apply the extended IB method to flow in a structured porous medium and focus on bulk properties such as the gradient of the average pressure and the Nusselt number. Reliable qualitative results were obtained with 16-32 grid points per singly-connected fluid region.*

1 INTRODUCTION

Compact heat exchangers play an important role in modern process industries¹. Predictions of heat and fluid flow through such devices are often hindered by the intricate internal geometries adopted in “improved-efficiency” product designs. Geometric details of the inner structures, such as size, shape and tortuosity, are almost impossible to capture with standard numerical methods employing body-conforming grids. In this paper, we present a volume-penalizing immersed boundary (IB) method² to approximate the flow of fluid around geometrically complex solid bodies. The volume-penalizing form of the IB method utilizes a phase-indicator function, operating on a Cartesian grid, to distinguish grid cells occupied by a fluid or by a solid. This solid-body approximation allows the IB method to be very flexible in its input geometry; allowing for geometrical data from various sources, e.g., computed tomography imaging. An extension on the basic IB method is made to include coupled fluid-solid heat transfer. Two test-cases are presented to validate the method: The first is laminar flow between two parallel walls, and the second is flow through a structured porous medium composed of an inline-arrangement of square cylinders.

IB methods can be used to predict the flow around arbitrarily shaped solid bodies using nonbody-conforming grids². Solid bodies are embedded on a Cartesian grid and boundary conditions are imposed by applying forces near the solid interface. These forces approximate the no-slip condition. Fluid-solid energy interaction is taken into account using a unified treatment of the energy transport equation, and is based on a single continuous temperature field throughout the entire computational domain. We solve the advection-diffusion equation for the temperature. In the fluid domain, both advection and diffusion are active components of transport. However, in the solid domain, the velocity field is zero and only diffusion is active. Jumps in the physical properties from one phase to the other (e.g., the thermal diffusivity) are tracked using the phase-indicator function. Care is taken to ensure a continuous heat-flux across the fluid-solid interface, as the temperature gradient is discontinuous at this interface. The accuracy of the proposed IB method is investigated in detail for the cases of laminar channel flow and flow through an inline-arrangement of square rods. Reliable solutions are obtained using about 16-32 grid cells across singly-connected openings in the fluid domain.

The structure of this paper is as follows. We formulate the IB method in Sec. 2 and turn to the extension toward conjugate heat transfer subsequently in Sec. 3. The application to laminar forced-convection problems is discussed in Sec. 4 and, finally, concluding remarks are collected in Sec. 5.

2 AN IMMERSSED BOUNDARY METHOD FOR SIMULATING FLOW AROUND SOLID OBJECTS

In this section we briefly introduce the governing equations of momentum transport and the forcing strategy behind the volume-penalizing IB method.

The equations that govern the motion of an incompressible fluid are the Navier-Stokes equations³:

$$\nabla \cdot \mathbf{u} = 0, \quad (1a)$$

$$\frac{\partial \mathbf{u}}{\partial t} + \mathbf{u} \cdot \nabla \mathbf{u} = -\frac{1}{\rho} \nabla p + \nu \nabla^2 \mathbf{u} + \mathbf{f}. \quad (1b)$$

The first equation represents the conservation of mass (at constant fluid mass-density), and the second the conservation of momentum. Variables in the system are: the fluid velocity vector $\mathbf{u} = (u, v, w)^T$, the fluid mass-density ρ , the pressure p , the kinematic viscosity $\nu = \mu/\rho$ with molecular viscosity μ , and a body force per unit mass \mathbf{f} . The vector differential operator is given by the symbol $\nabla \equiv (\partial/\partial x, \partial/\partial y, \partial/\partial z)^T$, and correspondingly, the Laplace operator by $\nabla^2 \equiv \nabla \cdot \nabla$.

When simulating the flow of fluid around solid bodies Eq. (1) is accompanied by no-slip boundary conditions (i.e., $\mathbf{u} = 0$) along all fluid-solid interfaces. These boundary conditions, internal to the computational domain, pass on information to the “fluid-parcels” on the presence of solid bodies. In cases where these boundaries are complex geometrical objects, the construction of a body-conforming grid of high quality is a challenging and time-consuming process. In the IB method, the internal boundary conditions are replaced by a source term (or forcing function) in the momentum equation that reproduces approximately the effect of the original no-slip condition²; particularly, that solid bodies are impervious to the fluid. This approach to enforcing boundary conditions is particularly helpful when simulating flows around solid bodies too complex to mesh in most engineering environments. In these cases, the IB method, using a Cartesian grid, provides a practicable alternative by approximating a solid body through the forcing strategy. Additionally, uniform Cartesian grids allow for the use of very efficient numerical methods.

Various forcing strategies are available for the IB method². In this work we adopt a simple volume-penalizing strategy, where:

$$\mathbf{f} \equiv -\frac{1}{\epsilon} \Gamma(\mathbf{x})(\mathbf{u} - \mathbf{u}_s), \quad (2)$$

with \mathbf{u}_s a prescribed solid body velocity, $\epsilon \ll 1$ a sensitivity parameter, and Γ a phase-indicator function. The binary function Γ identifies regions in space occupied by a solid body, i.e., if \mathbf{x} is a point within the solid body: $\Gamma(\mathbf{x}) = 1$ (otherwise, $\Gamma(\mathbf{x}) = 0$ for \mathbf{x} not in the solid). In other words, the forcing is absent in regions occupied by the fluid; these regions are governed by the Navier-Stokes equation. In regions occupied by solid bodies the various fluxes in the momentum equation are dominated by the IB forcing, and deviations of the solid velocity \mathbf{u} from \mathbf{u}_s are quickly forced back to a negligibly small value. A sufficiently small value of ϵ will result in a narrow region near the fluid-solid interface where the velocity quickly reduces to the prescribed \mathbf{u}_s . An advantage of using the volume-penalizing form is that the forcing of the no-slip condition occurs over the

entire solid body, allowing for a continuous description of the velocity vector \mathbf{u} throughout the entire computational domain. This feature greatly simplifies the implementation of this IB method into an existing CFD solver, as information on all solid-body locations is included in Γ .

The equations of motion resulting from the IB formulation are treated numerically. We adopt a finite-volume discretization that preserves the skew-symmetry of the nonlinear convective fluxes and the positive-definite dissipative nature of the viscous fluxes⁴. A second-order accurate method for these fluxes is employed, implemented on a staggered grid. The effect of these fluxes is integrated in time using an explicit time-stepping algorithm of Adams-Bashforth type⁴. The contribution of the forcing term \mathbf{f} is integrated implicitly in time, which overcomes severe stability problems that would arise with explicit methods as $\epsilon \ll 1$.

In the following section our aim is to extend on the basic IB method to incorporate conjugate heat transfer between fluid-solid systems. We motivate the need for a single, continuous temperature field throughout the entire domain, i.e., in both the fluid and the solid parts of the domain. Subsequently, we introduce a discretization of this system which preserves continuity of the heat-flux vector. Note, the method is developed for and applied to the temperature equation, however, generally it is applicable to any advection-diffusion equation (e.g., species transport).

3 SINGLE-TEMPERATURE REPRESENTATION FOR COUPLED SYSTEMS

Many engineering problems involve complex physical interactions between its various components, e.g., conjugate heat transfer. On first inspection one is tempted to introduce separate temperature fields in the fluid and in the solid domains. Such an approach would require a careful distinction of the fluid and solid parts of the domain and a proper mesh generation near their interface. It is, however, possible to extend the basic IB method as outlined in the previous section to work with a single temperature field; which is consistent with the IB formulation for fluid flow. In particular, the transport equation for the thermal energy in each of the fluid and solid phases is given by (assuming constant thermal properties):

$$(\rho c_p)_f \left[\frac{\partial T_f}{\partial t} + \mathbf{u} \cdot \nabla T_f \right] = \lambda_f \nabla^2 T_f, \quad (3a)$$

$$(\rho c_p)_s \frac{\partial T_s}{\partial t} = \lambda_s \nabla^2 T_s, \quad (3b)$$

where a subscript f refers to the fluid part and s to the solid part of the domain. In solid parts of the domain we allow only diffusive transport, while advection and diffusion are considered to be important in the fluid parts. The thermal properties of each phase are given by the specific heat capacity c_p (at constant pressure) and the thermal conductivity λ .

The temperature distribution in the entire domain can be expressed more concisely in terms of a single temperature field T that satisfies:

$$\frac{\partial T}{\partial t} + \mathbf{u} \cdot \nabla T = \nabla \cdot (\alpha \nabla T), \quad (4)$$

where $\alpha \equiv \lambda/(\rho c_p)$ is the thermal diffusivity, and

$$\alpha = (1 - \Gamma)\alpha_f + \Gamma\alpha_s; \quad (5)$$

with $\alpha_f = \lambda_f/(\rho c_p)_f$ and $\alpha_s = \lambda_s/(\rho c_p)_s$. Consistent with the volume-penalization method for the momentum equation, the convective term in Eq. (4) vanishes within stationary solid bodies (as $\mathbf{u}_s = 0$). The temperature field T approximates T_f in the fluid parts of the domain and T_s in the solid parts. It is such that the energy transport is a continuous function of the spatial coordinate. In particular, this implies that $\alpha \nabla T$ is a continuous vector field, implying jumps in the components of the gradient of the temperature at locations where the thermal diffusivity is discontinuous, e.g., at fluid-solid interfaces. This property is central to the single-temperature formulation and needs to be fully incorporated into the discretization of Eq. (4).

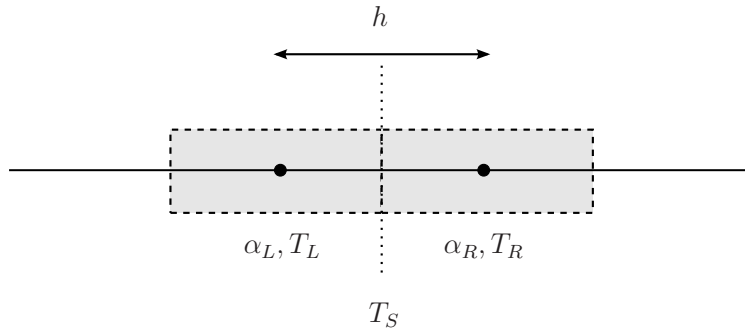


Figure 1: Discretization of the temperature gradient at a control-surface with a jump in the thermal property α . The auxiliary temperature T_S , a weighted average between T_L and T_R , facilitates the computation of the temperature gradient at interfaces between control-volumes of different thermal properties. The distance between the centers of adjacent control-volumes is denoted by h .

The numerical approach for the temperature equation is based on a simple finite-volume approach, with the additional property that the flux of energy through any control-surface is a continuous function of \mathbf{x} . The main idea may concisely be formulated in one spatial dimension (cf. Fig. 1). Continuity of the energy-flux may be expressed as $\alpha_L T'_L = \alpha_R T'_R$, where the prime denotes differentiation. In a finite-difference approximation this implies

$$\alpha_L T'_L \approx \alpha_L \frac{T_S - T_L}{\frac{1}{2}h} = \alpha_R \frac{T_R - T_S}{\frac{1}{2}h} \approx \alpha_R T'_R, \quad (6)$$

where we introduced the auxiliary variable T_S to denote the temperature at the surface between the adjacent “left” and “right” grid cells. From this expression we may solve for

T_S :

$$T_S = \frac{\alpha_L T_L + \alpha_R T_R}{\alpha_L + \alpha_R}. \quad (7)$$

For the case $\alpha_L = \alpha_R$ the surface temperature is simply the average of the left and right values. At jumps in α a suitable correction to T_S is obtained that maintains continuity of the energy-flux. Eq. (7) can be seen as a physically motivated surface-interpolation scheme for diffusive terms. This approach can readily be extended to two and three spatial dimensions. A further analysis of this type of approach is the subject of ongoing research and will be published elsewhere.

4 LAMINAR FORCED-CONVECTION OF HEAT AND FLUID IN PERIODIC DOMAINS

In this section we consider two test-cases of laminar forced convection of heat and fluid through domains with periodic boundary conditions. Both problems are solved using the extended IB method presented in the previous sections. The first test-case considers fully-developed channel flow. Numerical results for the velocity and temperature profiles are compared with their analytical counterparts. The second test-case considers a more complex inline-arrangement of squares. Results on the gradient of the average pressure and Nusselt number are compared with literature.

4.1 Forcing strategy for laminar flow in spatially periodic domains

In order to maintain a non-trivial flow in a spatially periodic domain an additional source term is required in the equations for momentum and heat flow. These terms compensate for the momentum and heat transfer at the fluid-solid interfaces. We incorporate the source terms as follows:

$$\nabla \cdot \mathbf{u} = 0, \quad (8a)$$

$$\frac{\partial \mathbf{u}}{\partial t} + \mathbf{u} \cdot \nabla \mathbf{u} = -\frac{1}{\rho} \nabla p + \nu \nabla^2 \mathbf{u} + \mathbf{f} - \frac{1}{\rho} \nabla P, \quad (8b)$$

$$\frac{\partial T}{\partial t} + \mathbf{u} \cdot \nabla T = \nabla \cdot (\alpha \nabla T) - S, \quad (8c)$$

$$S = (1 - \Gamma)S_f - \Gamma S_s. \quad (8d)$$

Momentum forcing is realized through the introduction of a mean pressure gradient ∇P . The source terms in the temperature equation are conveniently expressed as integrals of ∇T over the surface of control-volumes which coincide with the fluid-solid interface:

$$S_f \equiv \frac{1}{V_f} \int_{A_{sf}} \lambda_f \nabla T_f \cdot \mathbf{n} \, dA, \quad (9a)$$

$$S_s \equiv \frac{1}{V_s} \int_{A_{sf}} \lambda_s \nabla T_s \cdot \mathbf{n} \, dA; \quad (9b)$$

where \mathbf{n} is the unit-normal vector pointing away from the fluid into the solid, and $\{V_f, V_s\}$ the size of the fluid and solid control-volume, respectively. In periodic domains with flow dominated by viscous contributions, a good approximation can be obtained if the above is re-interpreted such that A_{sf} is the *total wetted surface area* in the whole domain, and V_f is the volume occupied by the fluid phase and V_s by the solid phase. Here, we restrict to such laminar flows and illustrate the approach on the basis of this more robust “domain-averaged” formulation. The comparison with a fully local formulation will be compiled in a forthcoming paper, showing the range of Reynolds numbers for which the domain-averaged version is an accurate approximation.

4.2 Fully-developed channel flow

To validate the extended IB approach, we consider fully-developed laminar flow in an infinitely long channel bounded by two parallel walls at $y = \{0, H\}$, see Fig 2(a). The walls are kept at a constant temperature T_w , and the initial fluid temperature is T_0 . We wish to compute the steady state velocity and temperature profiles in the channel by solving Eq. (8) and compare this with the analytical solution. The steady state Nusselt number ($\text{Nu} = h_{sf}H/\lambda_f$) is also computed analytically and compared with the numerical prediction. In order to apply the wall temperature boundary condition T_w with the IB method we will extend the channel domain to incorporate solid grid cells. Before proceeding with the numerical predictions we first derive the analytical solution.

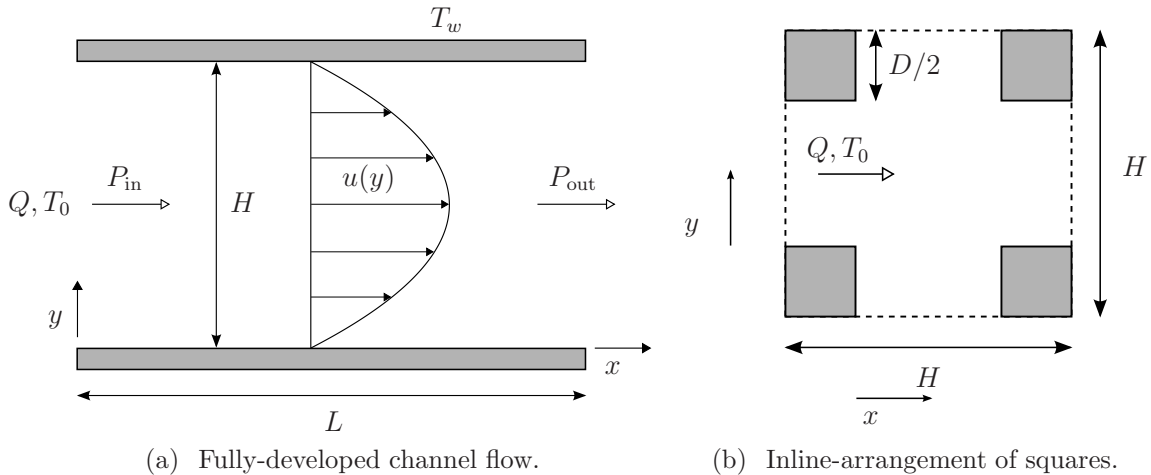


Figure 2: Test cases for the extended IB method: in (a) flow in a channel is shown with a pressure drop of $P_{\text{out}} - P_{\text{in}}$ over a length L , corresponding to a flow-rate Q . In (b), a unit-volume for a periodic inline-arrangement of square cylinders.

4.2.1 Analytical solution

Under the assumptions of steady, unidirectional flow, and also assuming vanishing gradients in the $\{x, z\}$ -directions, the transport equations reduce to the following set of ordinary differential equations:

$$\frac{d^2 u}{dy^2} = \frac{1}{\mu} \frac{dP}{dx}, \quad (10a)$$

$$\frac{d^2 T_f}{dy^2} = \frac{1}{\lambda_f} S_f, \quad (10b)$$

with boundary conditions $u(0) = u(H) = 0$ and $T_f(0) = T_f(H) = T_w$. Eq. (10a) is the well-known equation governing Poiseuille flow between two parallel plates⁵. The direction of flow is taken in the positive x -direction, for which the pressure drop $dP/dx < 0$. We assume the initial temperature to be such that $T_0 < T_w$, resulting in a transfer of energy into the fluid ($S_f > 0$). Integrating Eq. (10) twice over the channel height and applying the boundary conditions gives the following solutions:

$$u(y) = \frac{1}{2\mu} \frac{dP}{dx} (y^2 - Hy), \quad (11a)$$

$$T_f(y) = \frac{1}{2\lambda_f} S_f (y^2 - Hy) + T_w. \quad (11b)$$

A closing relation for the source term S_f follows from a property of the forcing strategy, that the energy content of each phase remains constant in time. Therefore, the volume-average of the fully-developed temperature field $\langle T_f \rangle = T_0$, i.e.,

$$\langle T_f \rangle = \frac{1}{V_f} \int_{V_f} T_f dV = T_0. \quad (12)$$

Substituting Eq. (11b) into the above equation and solving for S_f yields:

$$S_f = -\frac{12\lambda_f(T_0 - T_w)}{H^2}. \quad (13)$$

The equation for the fluid temperature now becomes:

$$T_f(y) = -\frac{6(T_0 - T_w)}{H^2} (y^2 - Hy) + T_w. \quad (14)$$

The Nusselt number $\text{Nu} = h_{sf}H/\lambda_f$ requires computing the heat transfer coefficient h_{sf} :

$$h_{sf} = \frac{\int_{A_{sf}} \lambda_f \nabla T_f \cdot \mathbf{n} dA}{A_{sf} (\langle T_s \rangle - \langle T_f \rangle)} = -\frac{\lambda_f}{T_w - T_0} \left. \frac{dT_f}{dy} \right|_{y=0} = \frac{6\lambda_f}{H}, \quad (15)$$

where dT_f/dy is taken from Eq. (14). Then:

$$\text{Nu} = 6. \quad (16)$$

4.2.2 Numerical approximation

To simulate an infinite laminar channel, we consider a cubic section of channel of dimension H^3 and extend the computational domain periodically along the $\{x, z\}$ -directions. Simulations are carried out using the dimensionless form of Eq. (8) based on the volume-averaged velocity $|\langle \mathbf{u} \rangle|$, the channel height H , the fluid thermal conductivity λ_f , and the fluid volumetric heat capacity $(\rho c_p)_f$ as reference scales. The temperature T is made dimensionless according to

$$\tilde{T} = \frac{T - T_0}{T_w - T_0}, \quad (17)$$

where the tilde denotes a dimensionless variable. The solid wall temperature is kept at a constant temperature T_w (i.e., $\tilde{T}_s = 1$) through the combination of a large thermal conductivity ratio λ_s/λ_f and the forcing S . With periodic conditions in the flow direction the momentum equation is forced by specifying a constant flow-rate Q in the x -direction such that $\langle \tilde{u} \rangle = 1$. This condition is then translated into an appropriate pressure gradient $d\tilde{P}/d\tilde{x}$. The Reynolds number is set to $\text{Re} = |\langle \mathbf{u} \rangle|H/\nu = 1$, and the Prandtl number is set to $\text{Pr}_f = \nu/\alpha_f = 1$; where α_f is the thermal diffusivity of the fluid. Experimentation has revealed an appropriate value for the sensitivity parameter $\epsilon = 10^{-10}$ (values of $\epsilon \leq 10^{-8}$ will suffice).

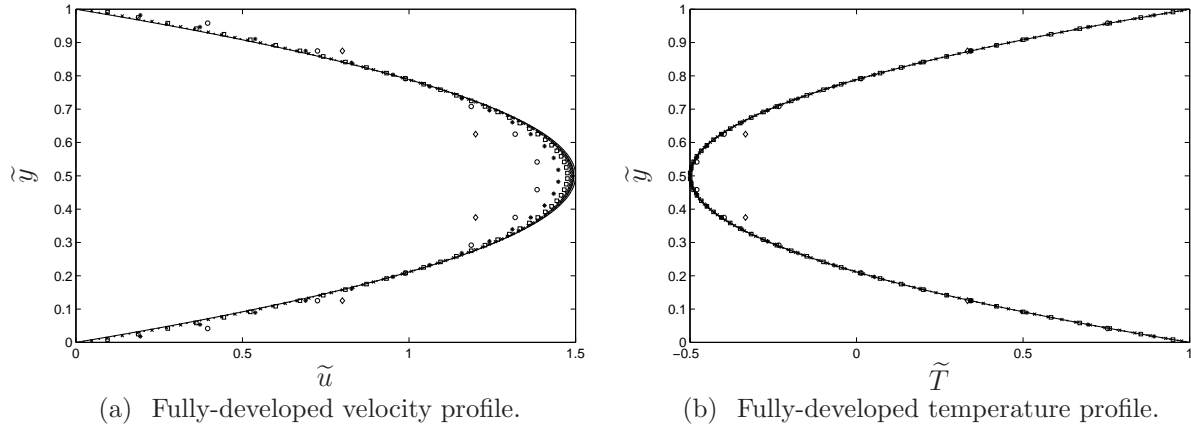


Figure 3: Numerical approximation of the fully-developed velocity and temperature as a function of the channel height $\tilde{y} \in [0, 1]$ and the grid resolution (n_y). The resolution is indicated by the markers: (\diamond) $n_y = 8$, (\circ) $n_y = 16$, ($*$) $n_y = 32$, (\square) $n_y = 64$, (\times) $n_y = 128$, and (\bullet) $n_y = 256$.

In Fig. 3 simulation results on the fully-developed (dimensionless) velocity and temperature profiles at various grid resolutions are compared with the analytical solution. The grid resolution ranges from $n_y = 2^k$ for $k = 3, \dots, 8$ in the y -direction. We simulate the solid wall temperature T_s (to represent a constant temperature T_w) using two computational nodes in both the upper and lower wall segments (amounting to four nodes for the solid phase). The number of nodes dedicated to simulating the fluid phase is therefore

$n_y - 4$. It is evident by comparing Fig. 3(a) with Fig. 3(b) that the velocity field exhibits a much slower convergence to the analytical solution. The order of convergence becomes clear from Fig. 4, where the norm of the difference between the computed value $\{\tilde{u}_h, \tilde{T}_h\}$ and the analytical solution $\{\tilde{u}, \tilde{T}\}$ is plotted:

$$\|\tilde{u}_h - \tilde{u}\|_{\ell^2(0,1)} = \sqrt{\sum_i (\tilde{u}_h(i) - \tilde{u})^2}, \quad (18)$$

$$\|\tilde{u}_h - \tilde{u}\|_{\ell^\infty(0,1)} = \max_i |\tilde{u}_h(i) - \tilde{u}|; \quad (19)$$

with $3 \leq i \leq n_y - 2$ the index of the computational node in the y -direction. For the velocity simulations: $\|\tilde{u}_h - \tilde{u}\|_{\ell^2(0,1)} \approx \mathcal{O}(\Delta y^{1/2})$ and $\|\tilde{u}_h - \tilde{u}\|_{\ell^\infty(0,1)} \approx \mathcal{O}(\Delta y)$, with Δy the grid width in the y -direction. For the temperature simulations: $\|\tilde{T}_h - \tilde{T}\|_{\ell^2(0,1)} \approx \mathcal{O}(\Delta y^{3/2})$ and $\|\tilde{T}_h - \tilde{T}\|_{\ell^\infty(0,1)} \approx \mathcal{O}(\Delta y^2)$. The approximate linear convergence rate in the velocity is due to the fact that the velocity field does not satisfy the no-slip condition at the solid boundary when use is made of the current formulation. This condition is actually satisfied a half grid width into the solid. An alternative approach in which the solid wall is shifted by half a grid cell to enforce the no-slip condition exactly, shows an improved convergence rate by one order; the extension of this to more complex domains is a topic of ongoing research.

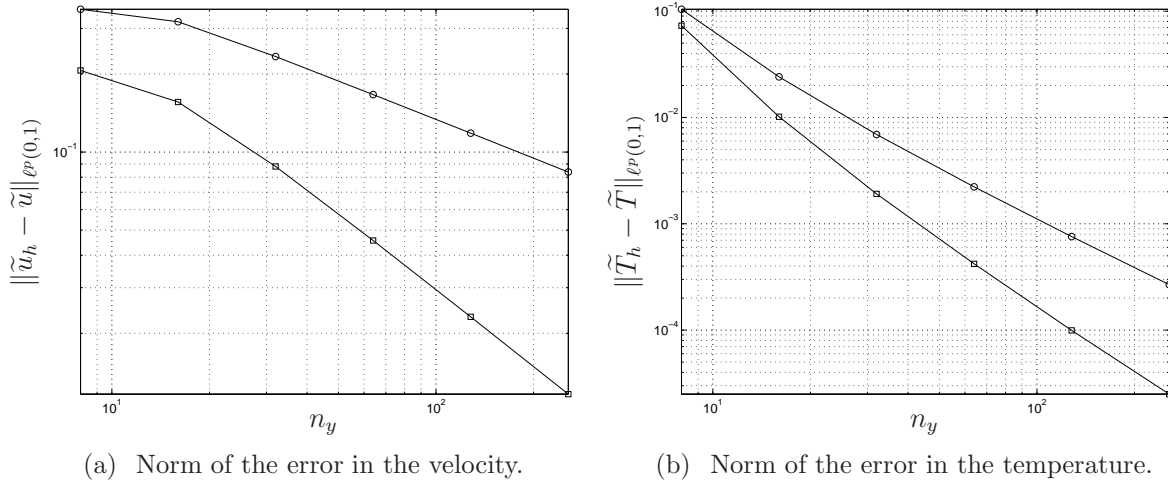


Figure 4: Norm of the error in the velocity $\|\tilde{u}_h - \tilde{u}\|_{\ell^p(0,1)}$ and the temperature $\|\tilde{T}_h - \tilde{T}\|_{\ell^p(0,1)}$ as a function of the grid resolution (n_y), with $p = \{2, \infty\}$. The ℓ^2 -norm is indicated by the (o)-markers, and the ℓ^∞ -norm by the (□)-markers.

The temperature field can also be processed to extract the heat transfer coefficient [cf. Eq. (15)], or in its dimensionless form, the Nusselt number ($\text{Nu} = h_{sf}H/\lambda_f$). Table 1 indicates the approximate Nusselt number Nu_h as a function of the grid resolution n_y . The analytical value for the Nusselt number is $\text{Nu} = 6$. The convergence of the numerical predictions is consistent with a second-order accurate method.

n_y	Nu_h	$\text{Nu} - \text{Nu}_h$
8	5.332869	$6.671308 \cdot 10^{-1}$
16	5.917590	$0.824105 \cdot 10^{-1}$
32	5.984637	$0.153630 \cdot 10^{-1}$
64	5.996624	$0.033764 \cdot 10^{-1}$
128	5.999198	$0.008020 \cdot 10^{-1}$
256	5.999800	$0.001996 \cdot 10^{-1}$

Table 1: Nusselt number (Nu_h) approximation as a function of the grid resolution (n_y). The analytical Nusselt number for laminar forced-convection in a channel with isothermal wall temperature is $\text{Nu} = 6$ [cf. Eq.(15)].

4.3 Inline-arrangement of squares

Consider macroscopically uniform flow along the x -axis (i.e., the volume-averaged velocity $\langle u \rangle$ is constant) through a model porous medium with a unit-volume as indicated by Fig. 2(b). The solid bodies are square cylinders of size D (within the unit-volume of size $D/2$) in a domain having square dimensions $H \times H$. We maintain a fixed fluid volume-fraction (porosity) $\phi = 1 - (D/H)^2 = 3/4$ (i.e., $D = H/2$). The fluid has an initial temperature T_0 , and the solid bodies are maintained at a constant temperature T_w . Periodic boundary conditions apply along all vertical and horizontal planes. We solve the dimensionless form of Eq. (8) (with reference scales identical to the channel flow problem) for a range of Reynolds numbers $10^{-1} \leq \text{Re} = |\langle \mathbf{u} \rangle| H / \nu \leq 10^2$, and compare our results with those from Nakayama et al^{6,7}. A scalar “measure” for the quality of the simulated flow will be the gradient of the average pressure and the Nusselt number.

The fluid flow is forced numerically by specifying a fixed flow-rate Q in the x -direction such that $\langle \tilde{u} \rangle = 1$ (where the tilde denotes a dimensionless variable). The required linear pressure gradient ($d\tilde{P}/d\tilde{x}$) is then computed to satisfy Q at each time-step. For all the conducted simulations the Prandtl number $\text{Pr}_f = \nu/\alpha_f = 1$, where α_f is the thermal diffusivity of the fluid. The solid wall temperature is maintained at a constant T_w through a similar approach as in the channel flow problem. For the porosity $\phi = 3/4$, the solidity, i.e., solid volume-fraction, is 25% of the total volume. Therefore, 25% of the computational nodes are dedicated to the solid domain and 75% of the nodes to the fluid domain. A grid resolution ($n_x \times n_y$) of 64×64 would result in 32 grid nodes dedicated to the “fluid-gap” at $\tilde{x} = 0$ [cf. Fig. 2(b)]. Simulation results for the dimensionless fully-developed velocity and temperature fields are plotted in Figs. 5 and 6 for two values of the Reynolds numbers $\text{Re} = \{1, 100\}$. At $\text{Re} = 1$, the velocity field slightly deviates from its bulk motion and flows into, and out of, the upper and lower cavities. By increasing the Reynolds number, two counter-rotating vortices develop, causing the bulk flow to resemble Poiseuille flow between two parallel plates. Notice how the IB method has forced the computational nodes within the solid domain to have a vanishing velocity.

The computed pressure field can be utilized to construct the gradient of the average

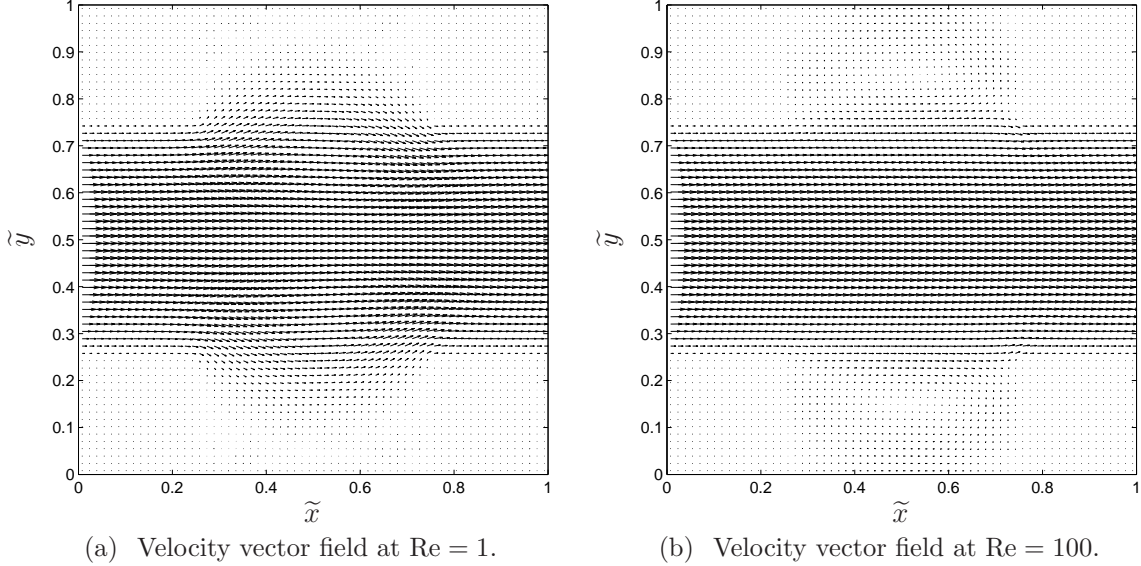


Figure 5: Simulation results of the fully-developed velocity for two values of the Reynolds numbers $Re = \{1, 100\}$. The grid resolution $(n_x \times n_y)$ is 64×64 , and the porosity $\phi = 3/4$. Flow is considered in the positive x -direction.

pressure^{6,7}:

$$-\frac{\partial \langle \tilde{p} \rangle}{\partial \tilde{x}} = \frac{1}{\mathcal{A}_x} \int_{\mathcal{A}_x} [\tilde{p}(1, \tilde{y}, \tilde{z}) - \tilde{p}(0, \tilde{y}, \tilde{z})] d\tilde{y}d\tilde{z}, \quad (20)$$

where \mathcal{A}_x is the surface area of the plane (per unit of length) through which the fluid enters or exits the unit-volume, i.e., $\mathcal{A}_x = 1 - \sqrt{1 - \phi} = 1/2$. The values of $-\partial \langle \tilde{p} \rangle / \partial \tilde{x}$ for various Reynolds numbers (Re) and grid resolutions $(n_x \times n_y)$ are shown in Table 2. A comparison is made with the numerical results of Nakayama et al.⁶ performed using a non-uniform, body-conforming grid. Convergence is seen with increasing grid resolution. In Fig. 7, the gradient of the average pressure is plotted for a range of Reynolds numbers and three grid resolutions. The solid line represents the macroscopic model known as the Forchheimer extended Darcy equation. The coefficients in this equation are found numerically by Nakayama et al.^{6,7}.

$(n_x \times n_y) \setminus Re$	10	100	600
181×181 (Nakayama et al. ⁶)	7.82	0.835	0.154
32×32	6.65	0.711	0.124
64×64	7.16	0.768	0.135
128×128	7.45	0.800	0.143

Table 2: Effect of grid resolution $(n_x \times n_y)$ on the gradient of the average pressure $(-\partial \langle \tilde{p} \rangle / \partial \tilde{x})$ for three values of the Reynolds number $Re = \{10, 100, 600\}$. The boldfaced values represent results obtained by Nakayama et al.⁶ using a non-uniform, body-conforming grid.

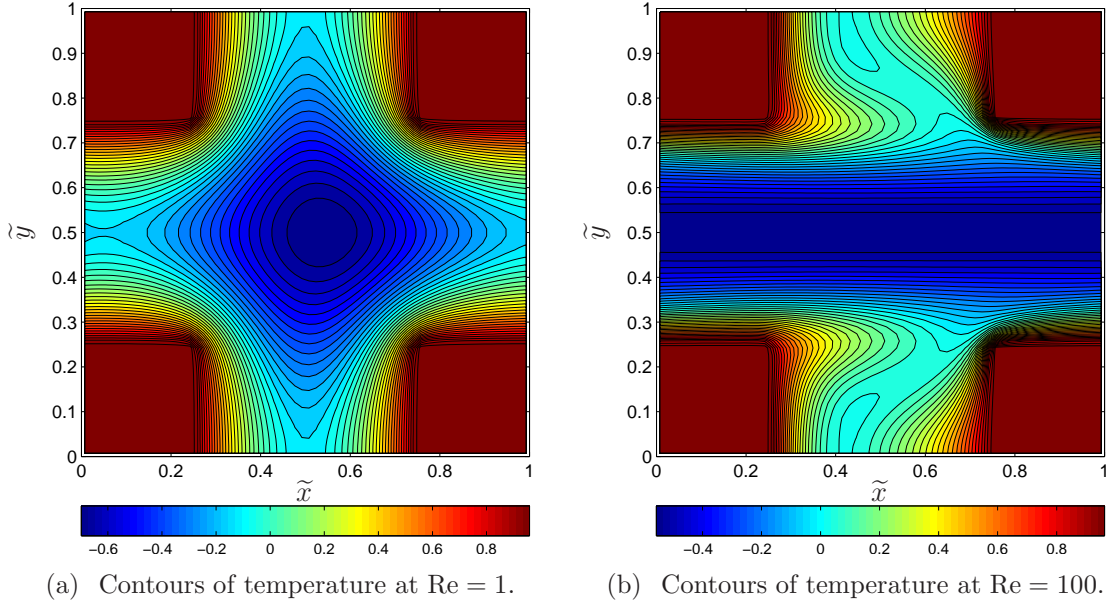


Figure 6: Simulation results of the temperature field for two values of the Reynolds numbers $Re = \{1, 100\}$. The grid resolution $(n_x \times n_y)$ is 64×64 , and the porosity $\phi = 3/4$.

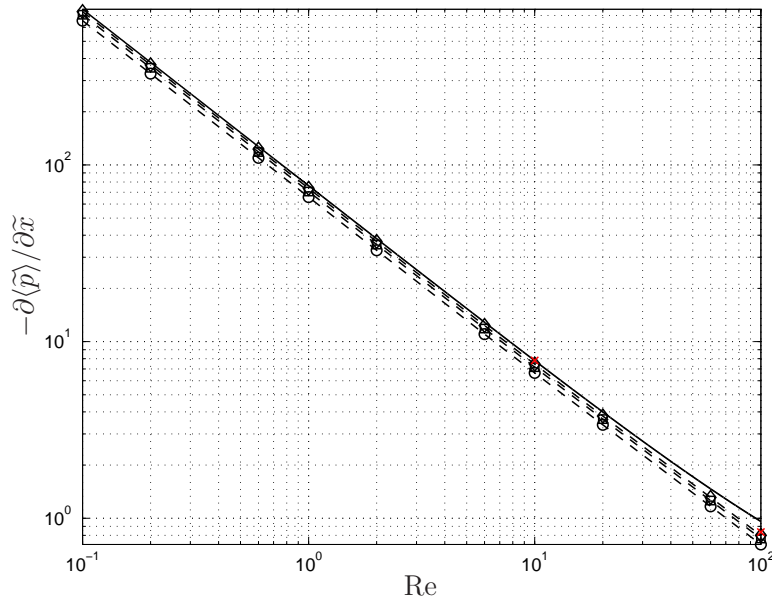


Figure 7: Simulation results ($\phi = 3/4$) for the gradient of the average pressure $(-\partial\langle\tilde{p}\rangle/\partial\tilde{x})$ as a function of the Reynolds number (Re) and the grid resolution $(n_x \times n_y)$. The resolution is indicated by the markers: (\circ) 32×32 , (\square) 64×64 , and (\diamond) 128×128 . The solid line is the Forchheimer extended Darcy equation as determined by Nakayama et al.^{6,7}. The (\times) -markers indicate the simulated values of Nakayama et al.⁶ in Table 2.

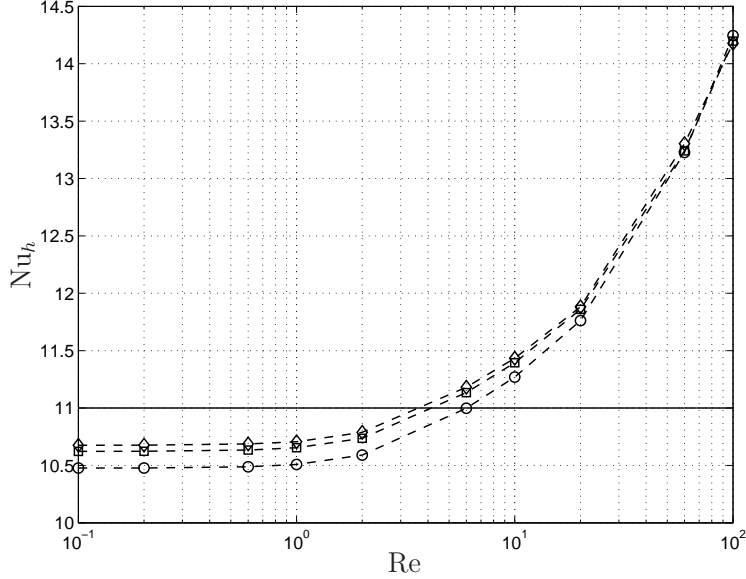


Figure 8: Simulation results ($\phi = 3/4$) for the Nusselt number (Nu_h) as a function of the Reynolds number (Re) and the grid resolution ($n_x \times n_y$). The resolution is indicated by the markers: (\circ) 32×32 , (\square) 64×64 , and (\diamond) 128×128 . The solid line represents the correlation proposed by Nakayama et al⁷.

The temperature field can also be utilized to construct the overall heat transfer coefficient:

$$h_{sf} = \frac{\int_{A_{sf}} \lambda_f \nabla T_f \cdot \mathbf{n} dA}{A_{sf} (\langle T_s \rangle - \langle T_f \rangle)}, \quad (21)$$

where A_{sf} is the total wetted surface area. In Fig. 8 the heat transfer coefficient, represented in dimensionless form by the Nusselt number ($Nu = h_{sf}H/\lambda_f$), is plotted for a range of Reynolds numbers and at three grid resolutions. Grid convergence is seen with increasing resolution. A comparison has also been made between our computed values for the Nusselt number and the proposed correlation of Nakayama et al⁷. Results seem to coincide for low values of the Reynolds number ($Re \leq 1$). However, with increasing Reynolds number, our results increase monotonically. The probable cause of this discrepancy is the different forcing strategy that was adopted for the energy equation. Our approach uses a domain-averaging strategy (cf. Sec. 4.1), possibly smearing out small-scale details in the temperature field which can have an affect on the overall heat transfer characteristics. This affect is minimized for the viscous flow regime. Further research will be necessary on this topic.

5 CONCLUDING REMARKS

We have presented a volume-penalizing immersed boundary (IB) method for approximating the flow of fluid around solid bodies. This method uses a nonbody-conforming (Cartesian) grid, and is suitable for flow problems involving geometrically complex solids.

No-slip boundary conditions are expressed through an added source term in the momentum equation of the fluid. This source term, or forcing function, acts only within the solid part of the domain, and prevents fluid from entering it. We have also presented an extension to the standard fluid dynamics to incorporate coupled fluid-solid heat transfer. A single convection-diffusion equation for the temperature has been introduced for the entire fluid-solid system. This equation reduces to diffusive transport in the solid due to a vanishing velocity field within this domain. Jumps in the physical properties of each phase are captured using a phase-indicator function borrowed from the volume-penalization methodology. Attention has been given at the discrete level to preserving the continuity of the energy flux across fluid-solid interfaces. An intermediate, surface temperature, was introduced at the interface between two grid cells which helps approximate the temperature gradient at this interface.

Using two test-cases, laminar channel flow and flow in a model porous medium, we have shown that the extended IB method can capture reliably heat and fluid transport. With sufficient grid resolution, about 16-32 grid points per “fluid gap,” much of the transport dynamics can be captured to give a reliable impression for laminar flow problems. Further research will be conducted on forcing strategies for the energy equation with periodic boundary conditions.

6 ACKNOWLEDGMENTS

The authors wish to thank Philip Morris International R&D for their financial support, and the Dutch Supercomputing Facility SARA. We also like to thank R.W.C.P. Verstappen of the University of Groningen for his contributions.

REFERENCES

- [1] J. E. Hesselgreaves, Compact Heat Exchangers: Selection, Design and Operation, *Elsevier Science Ltd.*, (2001).
- [2] R. Mittal and G. Iaccarino, Immersed Boundary Methods, *Annu. Rev. Fluid Mech.*, **37**, 239–261 (2005).
- [3] R. B. Bird, W. E. Stewart and E. N. Lightfoot, Transport Phenomena, 2nd Edition, *John Wiley & Sons Inc.*, (2002).
- [4] R. W. C. P. Verstappen and A. E. P. Veldman, Symmetry-Preserving Discretization of Turbulent Flow, *J. Comput. Phys.*, **187**, 343–368 (2003).
- [5] G. K. Batchelor, An Introduction to Fluid Dynamics, *Cambridge University Press*, (2000).
- [6] A. Nakayama, F. Kuwahara, T. Umemoto and T. Hayashi, Heat and Fluid Flow Within an Anisotropic Porous Medium, *J. Heat Transfer*, **124**, 746–753 (2002).

- [7] A. Nakayama, F. Kuwahara and T. Hayashi, Numerical Modelling for Three-Dimensional Heat and Fluid Flow Through a Bank of Cylinders in Yaw, *J. Fluid Mech.*, **498**, 139–159 (2004).